Materials Science & Engineering B 260 (2020) 114615

Contents lists available at ScienceDirect

Materials Science & Engineering B

journal homepage: www.elsevier.com/locate/mseb

Anisotropic optical phonons in MOCVD grown Si-doped GaN/Sapphire epilayers

Devki N. Talwar[a,b,*], Hao-Hsiung Lin[c], Zhe Chuan Feng[d,e,*]

[a] Department of Physics, University of North Florida, 1 UNF Drive, Jacksonville, FL 32224-7699, USA
[b] Department of Physics, Indiana University of Pennsylvania, 975 Oakland Avenue, 56 Weyandt Hall, Indiana, PA 15705-1087, USA
[c] Graduate Institute of Electronics Engineering and Department of Electrical Engineering, National Taiwan University, Taipei 10617, Taiwan, ROC
[d] Laboratory of Optoelectronic Materials & Detection Technology, Guangxi Key Laboratory for the Relativistic Astrophysics, School of Physical Science & Technology, Guangxi University, Nanning 530004, China
[e] State Key Laboratory of Luminescence and Applications, Changchun Institute of Optics, Fine Mechanics and Physics, Chinese Academy of Sciences, 130033 Changchun, China

ARTICLE INFO

Keywords:
Micro-Raman spectroscopy
MOCVD
Bond-orbital model
Lattice relaxation effect
Impurity-vibrational modes

ABSTRACT

Micro-Raman spectroscopy is employed to study the anisotropic optical phonons of Si-doped GaN/Sapphire epifilms grown by metal organic chemical vapor deposition method. In an undoped 3.6 μm thick sample – our polarized Raman measurements in the backscattering geometry revealed major first order modes of GaN and sapphire. Careful analyses of the second-order Raman spectra using critical-point-phonons from a rigid-ion-model fitted inelastic X-ray spectroscopy data with appropriate selection rules helped us attain expedient data for the lattice dynamics of GaN. In Si-doped films, a modified phonon confinement model is used for simulating Raman line shapes of E_2^{high} phonons to monitor crystalline quality. While the optical phonons in lightly doped samples are coupled to electron plasma– at higher carrier concentration the over-damped A_1(LO) mode vanished in the background. For each sample we assessed the transport parameters by simulating Raman profiles of A_1(LO) line shape with contributions from plasmon-LO-phonon and Lorentzian shaped E_g sapphire mode. A realistic Green's function theory is adopted to study the vibrational modes of Si donors and Mg acceptors in GaN by including force constant changes estimated from lattice relaxations using first-principles bond-orbital model. Theoretical results of impurity-activated modes compared favorably well with the existing Raman scattering data.

1. Introduction

In recent years, a dramatic boost of fundamental research for the wurtzite (wz) group III-Ns (AlN, GaN, InN) is driven by the successful fabrications of many electronic and optoelectronic devices [1–4]. Among several wide bandgap semiconductors, the benefits of using III-Ns are related to their exceptional electrical, structural and mechanical properties – crucial for designing the short-wavelength laser diodes, blue-green light-emitting diodes (LEDs), photocatalysts, detectors, sensors, high-temperature, high-power, high-frequency, high-density data storage devices for many energy applications and space-exploration needs [1–24].

Although the importance of GaN-based materials for electronic devices has been highlighted in various theoretical works [1–4] – the initial growth-related setbacks had posed huge obstacles for device fabrications. The major issues were associated with (*a*) the reproducibility of films morphology, (*b*) pervasive unintentional n-type conductivity, (*c*) lack of efficient p-type dopants, and (*d*) the absence of both native and/or lattice matched/thermally compatible substrates. The earlier growth of GaN on sapphire (Al_2O_3) resulted in high density of threading dislocations due to large disparity ($\sim -16\%$) in the lattice constants between epifilm and the substrate to cause impractically small critical layer thickness. As the coefficient of thermal expansion in basal plane of GaN is notably different from Al_2O_3 – the high temperature deposition process employed in the epitaxial growth of GaN/Sapphire epifilms also ensued thermal stress upon cooling.

Controlled growth with major improvements in crystalline quality of GaN/sapphire films has been achieved [24] by employing a two-step

* Corresponding authors at: Department of Physics, University of North Florida, 1 UNF Drive, Jacksonville, FL 32224-7699, USA (D.N. Talwar). Laboratory of Optoelectronic Materials & Detection Technology, Guangxi Key Laboratory for the Relativistic Astrophysics, School of Physical Science & Technology, Guangxi University, Nanning 530004, China (Z.C. Feng).

E-mail addresses: d.talwar@unf.edu (D.N. Talwar), fengzc@gxu.edu.cn (Z. Chuan Feng).

https://doi.org/10.1016/j.mseb.2020.114615
Received 31 December 2019; Received in revised form 14 June 2020; Accepted 29 June 2020
0921-5107/ © 2020 Elsevier B.V. All rights reserved.

metal–organic chemical vapor deposition (MOCVD) method. Earlier attempts of obtaining p-type GaN were equally futile until Nakamura et al. [25] demonstrated the activation of Mg acceptor by using post-growth thermal annealing to attain adequate free hole concentration. These breakthroughs have certainly helped fabricate [24–25] GaN-based p-n junctions followed by double heterostructures for creating the first LED with blue emission in candela scale. While the current and future needs of GaN-based quantum-well structures are quite assuring [1–24] – a large amount of work still needs to be done to improve the materials' basic characteristics for achieving its full capacity in device applications. One must note that the electronic transport, nonradiative electron relaxation process, lattice specific heat, structural and defect properties are all linked to device engineering and design. These traits can be strongly influenced by the lattice phonon excitations. One must note that there have been and still many challenges of growing large size wz GaN single crystals to obtain complete phonon dispersions by inelastic neutron-scattering. For using GaN in commercial applications [1–24] – it is equally important (*a*) to identify the nature of intrinsic and doped defects which cause deep traps, (*b*) to assess their influence on materials electrical and optical properties, and (*c*) to minimize their effects for optimizing device performance.

In order to probe the optical, structural and electrical attributes of intrinsic and doped GaN experimentally – it has been a routine practice to bring in a variety of characterization techniques viz., Raman scattering spectroscopy (RSS), [26–32] Fourier transformed infrared (FTIR) absorption, reflectivity and/or transmission measurements, [32] electron paramagnetic resonance (EPR), [33] deep-level transient spectroscopy (DLTS), [34,35] photoluminescence (PL), [36–41] etc. While RSS [26–31] is considered as one of the most compatible methods to study the vibrational properties in polar materials – its exploitation for characterizing donor and acceptor defects [42–47] in III-Ns has remained, however, surprisingly enigmatic. In n- and/or p-doped GaN, the magneto-transport (Van-der-Pauw or Hall) measurements are frequently used to acquire the free charge carrier concentration N and mobility μ [31,44] Being a purely optical method, the RSS has the potential to study not only the interactions of free carrier plasma [29,30] with lattice phonons for assessing N and μ but also examining residual stress states in epitaxially grown materials. One must note that for the implications of heteroepitaxial structures in device engineering – the residual stress/strain in epifilms plays an important role. While few attempts are made to understand the residual stress caused by lattice mismatch and/or thermal misfits – a highly desirable and systematic study for comprehending the evolution of stress caused by Si-doping in GaN/Sapphire films is either sparse and/or contradictory [45–47]. Limited Raman spectroscopy results [27,28] exist for studying the effects of Mg (acceptor), and Si (donor) defects on the lattice dynamics of epitaxially grown GaN. To the best of our knowledge, no localized vibrational modes (LVMs) of isolated substitutional defects (e.g., C_N, O_N, Si_{Ga}, Mg_{Ga}) are observed experimentally.

In this paper we have reported the results of a comprehensive experimental and theoretical study to examine the influence of Si defects on the vibrational and structural characteristics of high quality MOCVD grown GaN/Sapphire epifilms. A two-step process, employed here to prepare different Si-doped GaN/Sapphire epifilms, is succinctly outlined in Section 2.1. All the GaN/Sapphire samples (#S_1-#S_5) are characterized by secondary-ion-mass spectroscopy (SIMS), x-ray diffraction (XRD), FTIR, Hall effect and sheet resistivity methods to assess the film thickness d, charge carrier concentration N and mobility μ (see: Table 1). Room temperature (RT) micro-Raman scattering measurements are performed in the backscattering geometry to study the anisotropic optical phonons. A 514.5 nm line of Ar^+ ion laser is employed as an excitation source for observing the 1st order symmetry-allowed optical phonons as well as 2nd order combinations of acoustic/optical overtones (cf. Section 2.2). The study has helped us (cf. Section 3) (*a*) evaluate the crystalline quality of the samples, (*b*) assigning the observed Raman features (cf. Section 3.1) to the critical point phonons of GaN and sapphire, (*c*) estimate N and μ, and (*d*) deduce residual stress/strain in Si-doped GaN/Sapphire (cf. Section 3.2) epilayers. To monitor the quality of films, we also adopted meticulous theoretical methods (cf. Sections 3.2.1 and 3.2.2) to simulate Raman line shapes of E_2^{high} and A_1(LO) optical phonon modes. These calculations have assisted us to examine the stress/strain as well as assessing N and μ in GaN/Sapphire samples. Unlike many reports in the literature, our analysis of E_2^{high} Raman modes indicated insignificant residual strain caused by Si doping in GaN/Sapphire (cf. Section 3.2.2) in films having N less than $< 9.95 \times 10^{17}$ cm^{-3}. For isolated Si donors (d^+) and Mg acceptors (a^-) in GaN we have incorporated a realistic Green's function method by accurately including impurity-host interactions – estimated from a bond-orbital model (BOM) (cf. Section 3.2.3) to calculate the impurity-induced vibrational modes. Theoretical results are compared and/or contrasted against the existing Raman scattering data [27,28] with concluding remarks presented in Section 4.

Table 1
The charge carrier concentration N (10^{17}cm^{-3}), film thickness d (μm), and electron mobility (cm^2/V s) values obtained by different methods in the MOCVD grown Si-doped GaN/Sapphire samples (see: text).

Sample	N (10^{17}cm^{-3})			d (μm)		μ (cm^2/V s)		
	Hall	Fitted IR [a]	Raman [b]	XRD	Fitted IR [a]	Hall	Fitted IR [a]	Raman [b]
S_0 (undoped)	0.327			3.58	3.61			
S_1	3.58	3.36	3.72	2.43	2.47	295	295	383
S_2	6.57	9.07	8.83	1.94	1.95	227	225	272
S_3	4.85	5.10	5.20	1.99	2.00	268	265	330
S_4	7.65	11.2	9.95	2.03	2.05	209	207	243
S_5	2.77	2.87	3.08	1.62	1.67	374	384	410

[a] Ref. [64].
[b] This work.

2. Experimental

2.1. Metal organic chemical vapor deposition growth of n-GaN/Sapphire

By employing a two-step growth process, we have prepared high-quality samples (# S_1- S_5) of Si-doped GaN on (0001) oriented sapphire, using MOCVD technique. Following the methodology adopted earlier [30] we first created an ultrathin GaN buffer layer of about ~25 nm at low temperature (450 °C) on sapphire substrate (cf. Fig. 1) followed by depositing GaN films at high-temperature (1050 °C) of thickness d ranging between ~1.67 μm to 2.5 μm. Mono-silane (SiH_4) is used for transforming GaN films into n-type. A series of improved quality Si-doped GaN epifilms are prepared under the same growth conditions with SiH_4 flux systematically modulated for achieving different doping levels. All the MOCVD grown n-GaN/Sapphire samples were first characterized by SIMS and XRD methods [31] to estimate film thickness d. The values of free electron concentration N and mobility μ are derived from Hall effect, sheet resistivity and FTIR measurements. The Hall (FTIR) mobilities are found decreasing from 374 (384) cm^2/V s for N around ~2.77 (2.87) × 10^{17} cm^{-3} to 209 (207) cm^2/V s for N ~ 7.65 (11.2) × 10^{17} cm^{-3}. The estimated values of μ by Raman spectroscopy for Si-doped GaN/Sapphire epifilms with different charge carrier concentration fit reasonably well with theoretical results obtained from an empirical Caughey–Thomas [47] model (cf. Section 3.2.2). In our samples the mobility μ and free electron concentration N amounts to ≥90% of the total Si-concentration – suggesting a very low compensation ratio. A good quality of undoped GaN/Sapphire epifilm of thickness d ~ 3.6 μm (# S_o) is also prepared. This sample exhibited slightly n-type conducting behavior with N ~ 3.27 × 10^{16} cm^{-3} (cf. Table 1) due to the possible presence of residual oxygen (O) donors.

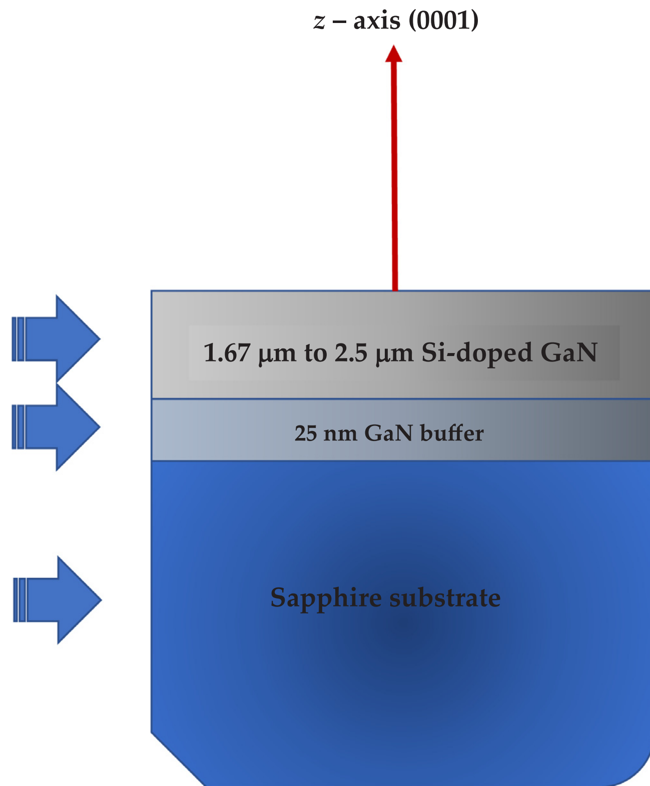

Fig. 1. Sketch of the basic structure of Si-doped GaN epifilms grown on sapphire substrate by using a two-step metal-organic chemical vapor deposition (MOCVD) technique (see text).

2.2. Raman scattering spectroscopy

We have undertaken comprehensive investigations using Raman scattering spectroscopy to assess the crystalline quality and critical-point-phonon energies in GaN/Sapphire epifilms. To perform the RT polarized micro-Raman measurements in the backscattering geometry with $Z(X,X)\bar{Z}$ and $X(Y,Y)\bar{X}$ or $Y(X,X)\bar{Y}$ configurations, we have employed a commercially available Renishaw-spectrometer equipped with rotation stage by utilizing an Ar^+ ion laser with 514.5 nm excitation source. The Raman equipment is outfitted with a microscope, a stigmatic single spectrograph (25-cm focal length), a holographic grating (1800 or 2400 grooves/mm), angle tunable band pass or notch filters, and a Peltier-cooled detector (576 × 384 pixels). The microscope lens employed here focused the laser beam on sample surface to a spot size of ~1 μm with output power of less than 1 mW – adjustable by neutral density filters. The dielectric beam splitter having reflection/transmission ratio of 30/70 for incident unpolarized light (λ = 514.5 nm) is used – playing two important roles: (*a*) directing laser light to the objective lens for excitation, and (*b*) delivering scattered light back to the spectrometer for detection. The spectral resolution of our Raman system is better than 1 cm^{-1} for collecting data in the infrared range.

3. Experimental results and theoretical analysis

Raman scattering spectroscopy is a contactless/nondestructive and very powerful technique for comprehending phonon characteristics of both undoped and doped semiconductors. In the perfect wz GaN crystal (see: Fig. 2 *a*)) there are two hexagonally close packed sublattices of Ga and N atomic species shifted against each other along the c-axis. An ideal structure with four atoms per unit cell belongs to a space group C_{6v}^4 ($P6_{3mc}$) [27]. At the center (i.e., $\vec{q} \simeq 0$ or **Γ**-point) of the Brillouin zone (BZ), the group theory predicts eight sets of phonon modes given by

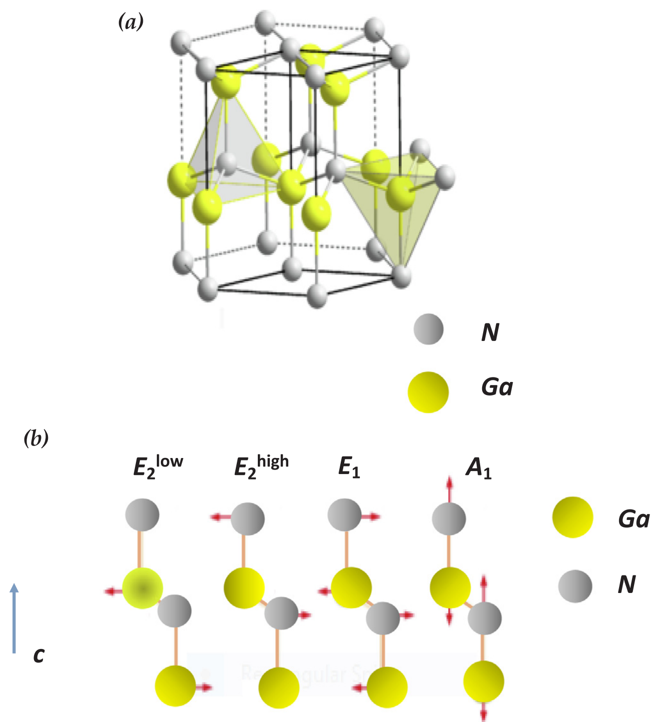

Fig. 2. (*a*) Sketch of the wurtzite GaN crystal structure. The size of spheres indicates the covalent radii – where the grey colored spheres represent nitrogen (N) atoms while the yellow colored sphere represent gallium (Ga) atoms. (*b*) The atomic displacements are represented of Γ-point of $E_2(E_2^{low}, E_2^{high})$, E_1 and A_1 phonons in the wurtzite GaN (see text). (For interpretation of the references to colour in this figure legend, the reader is referred to the web version of this article.)

$2A_1 + 2B_1 + 2E_1 + 2E_2$. While one set of A_1, E_1 optical vibrations are IR and Raman active – the second set is linked to the acoustic phonons. The two E_2-modes (E_2^{low}, E_2^{high}) are also Raman active (see: Fig. 2 *b*)) whereas the B_1 modes are silent i.e., neither IR nor Raman active. The E_2^{high} mode in GaN corresponds to atomic oscillations in the c-plane (see Fig. 2) having a nonpolar characteristic. Consequently, the E_2^{high} phonon frequency is sensitive to the residual in-plane stress. In n-GaN/Sapphire the stress can be evaluated from the observed shift of E_2^{high} mode with respect to a free standing GaN film. One must also note that the A_1 and E_1 vibrations split up into longitudinal optical LO (ω_{LO}^{A1} and ω_{LO}^{E1}) and transverse optical TO (ω_{TO}^{A1} and ω_{TO}^{E1}) components by macroscopic electric field (i.e., LO-TO splitting). This split affects the LO phonons to have higher energies than its TO counterparts i.e., $|\omega_{LO}^{A1} - \omega_{TO}^{A1}|$ and $|\omega_{LO}^{E1} - \omega_{TO}^{E1}| \gg |\omega_{LO}^{A1} - \omega_{LO}^{E1}|$ and $|\omega_{TO}^{A1} - \omega_{TO}^{E1}|$. In the heteroepitaxial growth of GaN, we have used sapphire substrate which exhibits seven Raman active phonon modes expressed by $2A_{1g} + 5E_g$.

3.1. Vibrational modes of GaN and sapphire

Vibrational properties of GaN/Sapphire epifilms are sensitive to the presence of intrinsic defects, strain, doping and growth temperature. While the lattice dynamics of bulk GaN is studied using phenomenological [48] and *ab-initio* methods [49] – the phonon dispersions are measured by inelastic X-ray scattering (IXS) [50]. The knowledge of phonon mode frequencies as well as their bandwidths are essential for extracting the information about the structural and dynamical characteristics of epitaxially grown materials. We used phonons from a realistic lattice dynamical scheme and assessed Raman phonon features in MOCVD grown n-GaN/Sapphire epifilms. As the momentum of incident and scattered photons are very small compared to the first BZ – only optical phonons near $\vec{q} \simeq 0$ are excited in the 1st order Raman

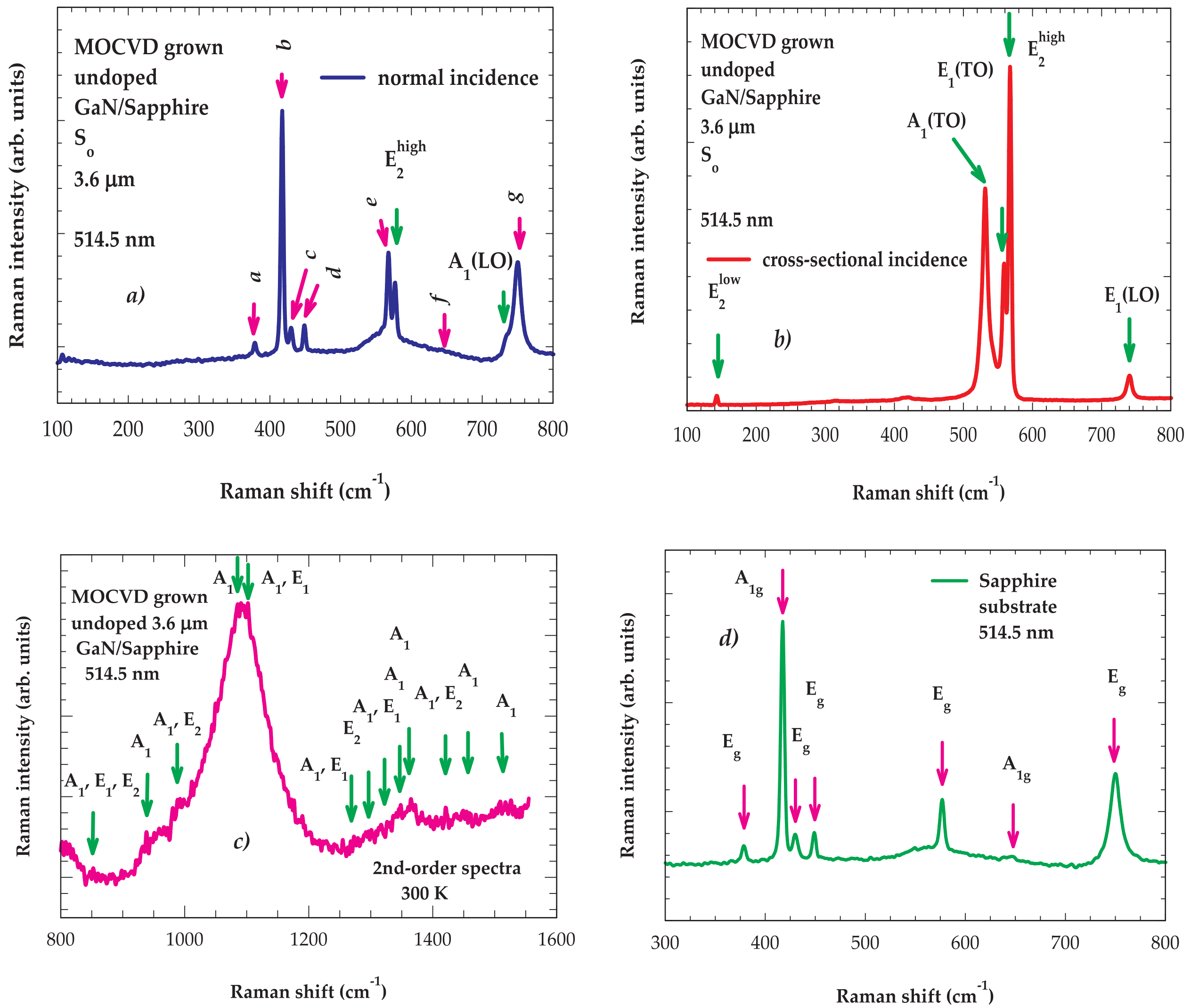

Fig. 3. Room temperature Raman spectra under the excitation of 514.5 nm in the backscattering geometry of an undoped GaN 3.6 μm thick epifilm grown on sapphire by using a 2-step MOCVD method : (*a*) The measured spectrum represents incident laser light used along the normal direction of the film, i.e., parallel to the c-axis of the wurtzite GaN. The features shown by letters *a* - *g* represent phonon modes of the sapphire substrate. (*b*) The Raman spectrum represents with incident laser light focused on the cross section of the film, i.e., perpendicular to the c-axis of the wurtzite GaN. (*c*) The spectrum displays second-order Raman results of the wurtzite GaN. (*d*) The spectrum shows results of Raman active modes of the sapphire substrate (see text).

process. Careful analysis of the 2nd order Raman spectra and examining the observed impurity and/or disorder induced phonon features helped us attain useful information about the lattice dynamics of GaN.

In Fig. 3 *a-b*) and *c*), we have displayed our RT results of RSS for an undoped ~3.6 μm thick GaN/Sapphire (sample # S_0) in the backscattering geometry by using a 514.5 nm excitation source. As GaN and sapphire materials are both semi-transparent to the visible wavelength – the Ar^+ ion laser is found adequate for extorting data of their lattice vibrations. From the 1st order Raman scattering, we have identified distinct phonon features of (wz) GaN when laser light is incident along the normal direction i.e., parallel to the c-axis of GaN (cf. Fig. 3 *a*)) and on the cross section of the film i.e., perpendicular to the c-axis of GaN layer (Fig. 3 *b*)), respectively. The experimental results of 2nd-order Raman spectra for the same sample are shown in Fig. 3 *c*) as well. Major Raman active modes observed for the sapphire substrate are also labelled in Fig. 3 *d*). In Table 2, we have listed the mode frequencies perceived in both 1st and 2nd order Raman spectra of the (wz) GaN film along with the 1st-order phonons determined for the sapphire substrate. All major Raman active modes observed in (wz) GaN epifilms and sapphire substrate have exhibited obeying apposite selection rules. The results of 2nd order Raman scattering experiments covering both the acoustic and optical overtone spectral regions are analyzed theoretically (cf. Table 2) by incorporating appropriate critical-point-phonon energies from the lattice dynamics of (wz) GaN and using group-theoretic selection rules. In addition, we have used the width and intensity of the 1st order Raman phonon lines to assess the quality of films (cf. Section 3.2) and the observed frequency positions for monitoring stress/strain in the epitaxially grown GaN/Sapphire samples.

3.2. Si-doped GaN/Sapphire

For Si-doped GaN/Sapphire epifilms, we reported results of experimental and theoretical study to comprehend the role of Si-dopants (cf. Section 3.2.1) and extricating charge carrier concentration *N* and mobility μ (cf. Section 3.2.2). In Fig. 4, the RT RSS results recorded in the backscattering geometrical configuration are displayed for five MOCVD grown GaN/Sapphire samples having different film thickness *d* and charge carrier concentration *N* (cf. Table 1). In each sample, the Fig. 4 revealed E_2^{high} and A_1(LO) optical phonon frequencies appearing between ~569 and 570 cm^{-1} and around ~740 cm^{-1}, respectively. While the E_2^{high} mode is considered sensitive to strain in GaN films – the A_1(LO) mode is, however, closely related to the charge carrier

Table 2
Room temperature Raman shifts, process and symmetry assignments of the experimental 1st and 2nd-order phonons in the backscattering geometry for an undoped (wz) GaN/Sapphire (sample # S_0). The frequencies of the observed Raman modes and their symmetry assignments are also identified for the sapphire substrate.

Experimental Raman shifts (cm^{-1}) and symmetry assignments							
(wz) GaN (1st order)		Sapphire (1st order)		(wz) GaN (2nd order)			
Our	Ref. [27]	Our	Ref. [49]	Our	Ref. [49]	Process	Symmetry
$142E_2^{low}$	$144E_2^{low}$						
					317	acoustic overtone	A_1
					410	acoustic overtone	A_1
		379 E_g	378 E_g				
		418 A_{1g}	418 A_{1g}		420	acoustic overtone	A_1, E_2
		431 E_g	432 E_g				
		450 E_g	451 E_g				
533 A_1(TO)	531.8 A_1(TO)				533	first-order process	A_1
560 E_1(TO)	558.8 E_1(TO)				560	first-order process	E_1
$569E_2^{high}$	$567.6E_2^{high}$				569	first-order process	E_2
		578 E_g	578 E_g				
		645 A_{1g}	645 A_{1g}		640	overtone	A_1
734 A_1(LO)	734 A_1(LO)				735	first-order process	A_1
742 E_1(LO)	741 E_1(LO)				742	first-order process	E_1
		750 E_g	751E_g				
				853	855	acoustic-optic comb.	A_1, E_1, E_2
				943	915	acoustic-optic comb.	A_1
				996	1000	acoustic-optic comb.	A_1, E_2
				1090,1105	1150	optic overtone	A_1
				1275,	1280	optic comb.	A_1, E_1
				1295	1289	optic comb.	E_2
				1330	1313	optic comb.	A_1, E_1, E_2
				1370	1385	optic overtone	A_1
				1425		optic overtone	A_1
				1462	1465	optic overtone	A_1
				1507	1495	optic overtone	A_1, E_2

Fig. 4. Room temperature Raman spectra of five (# S_1-S_5) different Si-doped GaN/Sapphire samples. The intensity of Raman shift for each sample is enhanced by a factor of ten between 700 and 800 cm^{-1} to highlight the asymmetric nature of the modes (see text).

concentration N. Consequently, one expects the LO-mode strongly interacting with electron plasma through electric field for instigating plasmon-LO-phonon (PLP) coupled modes. With increase of Si-doping, one anticipates shift in the asymmetric A_1(LO) peak position to cause broadening in the Raman line shape.

To highlight the nature of asymmetric A_1(LO) mode with different N we have amplified each spectrum of Si-doped GaN/Sapphire epifilms (cf. Fig. 4) by a factor of ten between the frequency range of ~ 700–800 cm^{-1}. In samples S_5 and S_1 with lower value of N, we noticed A_1(LO) phonon mode appearing around ~740 cm^{-1}. As N is increased, the phonon-plasmon coupling affected the A_1(LO) line shape – shifting Raman mode to higher frequency (see samples # S_2–S_4). Accordingly, the weak A_1(LO) mode in samples S_2 and S_4 vanished in the background and an E_g mode of sapphire near ~750 cm^{-1} became a dominant feature. By adopting meticulous theoretical models, we offered careful analyses of the observed Raman profiles for both E_2^{high} (in Section3.2. 1)and A_1(LO) (cf. Section 3.2.2) modes.

3.2.1. E_2^{high} mode

In polar materials, the physics of inelastic interaction of photons with lattice phonons is sensitive to internal and/or external perturbations [51–56]. Accurate analysis of the Raman profiles is crucial for assessing the distribution of nanostructured crystallites responsible for the observed asymmetric optical phonon line shapes. In the hetero-epitaxially grown n-GaN/Sapphire, the E_2^{high} mode is investigated by using a phonon confinement model (PCM). In this model we have simulated Raman intensity of optical modes by methodically integrating a line-shape function along with the correlation length L specifying the average size of materials' homogeneity region: [51–56]

$$I(\omega) = \int_0^1 \frac{|C(0,q)|^2 d^3q}{[\omega - \omega(\vec{q})]^2 + \left(\frac{\Gamma_0}{2}\right)^2} \quad (1)$$

where, $|C(0,q)|^2 = e^{-q^2L^2/4}$ is the Fourier coefficient with magnitude of wavevector $|\vec{q}\,|$ expressed in the units of $2\pi/a$; Γ s the natural line width (or full width at half maximum (FWHM)).

Owing to the energy and momentum conservation in GaN, the optical phonons near center of the BZ ($\vec{q} \simeq 0$) contribute to the Raman process. However, disorders and finite size defects may partially or completely relax momentum conservation rule leading either to the shifts and/or broadening of the Raman modes. Here, we have employed

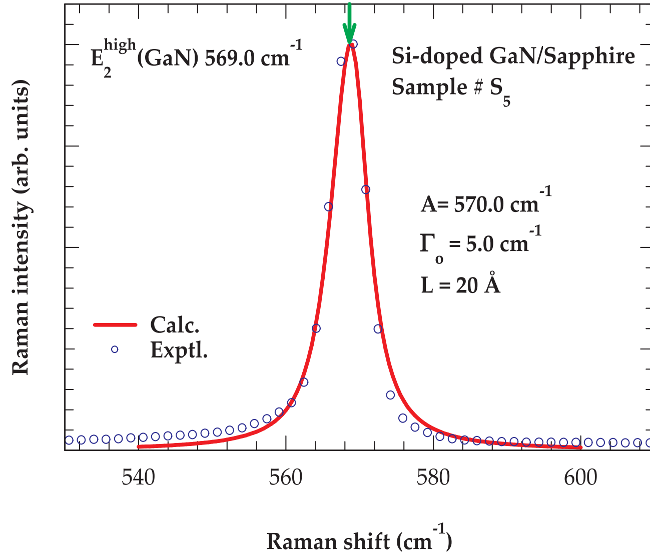

Fig. 5. The fitting of Raman scattering spectra of E_2^{high} mode for # S_5 sample (only) by using the phonon confinement model using Eq. (1). Similar calculations for other samples were also performed (not shown here) with required fitted parameter values reported in Table 3.

a PCM to simulate the Raman line shape of optical phonons in Si-doped GaN epifilms to assess the correlation length. According to Richter [51] the choice of $\omega(\vec{q})$ $[= A - B|\vec{q}|^2]$ is not imperative as long as it exhibits a parabolic behavior near the center of the BZ. The terms A and B are, respectively the adjustable parameters for determining the peak position and slope of the curve. By using Eq. (1), we have fitted the experimental E_2^{high} GaN modes of Si-doped GaN/Sapphire samples having different charge carrier concentration N. In Fig. 5, the experimental Raman line shape of sample # S_5 is displayed along with theoretical simulation. The values of A, L, B and Γ required to fit experimental data for all samples are reported in Table 3.

The comprehensive theoretical analyses have helped us optimize the growth parameters and to obtain relationship between crystalline quality and doping level. Based on our results we find (*a*) no appreciable shifts in the E_2^{high} mode frequencies – suggesting insignificant residual strain caused by Si doping in GaN at least in samples where the carrier concentration is less than $N < 9.95 \times 10^{17}$ cm^{-3}, and (*b*) the observed narrow FWHM of E_2^{high} Raman modes implying high structural quality of Si-doped GaN/Sapphire epilayers which has been well supported by XRD measurements [31]. Nonetheless, in an earlier report Lee et al. [57] suggested the possibility of relaxing compressive residual stress in Si-doped GaN/ Sapphire samples if N is increased up to $\sim 1.6 \times 10^{19}$ cm^{-3}. However, we have noticed that the authors (Ref. [57]) did not elaborate on the impact of Si-doping to report the shifts in the A_1(LO) phonons and/or coupled PLP modes (cf. Section 3.2.2) [58–62].

3.2.2. A_1 (LO) mode

In Si-doped GaN with free charge carrier concentration N, one expects the macroscopic electric field of the A_1(LO) mode to strongly interact with the collective excitation field of free carriers (i.e., plasmons) [58–61]. This interaction is responsible for producing two branches of the PLP modes. The nature of $L_\pm$ modes depends on plasmon frequency $\omega_P \left(\equiv \sqrt{\left(\frac{4\pi Ne^2}{\varepsilon_\infty m^*}\right)}\right)$ which is proportional to the square root of carrier concentration N. If the frequency of ω_P is smaller than that of an uncoupled A_1(LO) phonon ($\omega_P < \omega_L$) – the L_- mode behaves plasmon-like and L_+ acts as phonon-like. At higher N, when the frequency of ω_P becomes larger than A_1(LO) ($\omega_P > \omega_L$), the characteristic of L_+ mode changes from phonon-like to plasmon-like.

In doped materials with contributions from plasma ω_P and optical phonon frequencies (ω_L and ω_T), the dielectric function $\varepsilon(\omega)$ can be expressed as: [58]

$$\varepsilon(\omega) = \varepsilon_\infty \left[1 + \frac{(\omega_L^2 - \omega_T^2)}{(\omega_T^2 - \omega^2 - i\omega\Gamma)} - \frac{\omega_P^2}{(\omega^2 + i\omega\gamma)}\right] \quad (2)$$

where γ and Γ are their respective damping constants. Neglecting γ and Γ in Eq. (2), one can obtain the PLP modes $L_\pm$ from the roots of the equation

$$\omega_{L\pm}{}^2 = \frac{1}{2}\left\{\omega_L{}^2 + \omega_P{}^2 \pm [(\omega_L{}^2 + \omega_P{}^2)^2 - 4\omega_P{}^2\omega_T{}^2]^{\frac{1}{2}}\right\} \quad (3)$$

Clearly, Eq. (3) yields non-linear curves of $L_\pm$ modes as a function of N (see: Fig. 6 *a*) – showing a typical profile of the PLP-modes in n-GaN. In lightly doped samples with $N < 1.7 \times 10^{17}$ cm^{-3} –only A_1(LO) modes are observed [27,58–62]. As N increases one expects broadening of LO peak with a shift towards higher energy side. When N is increased between 4.85×10^{17} cm^{-3} to 7.65×10^{17} cm^{-3} – our Raman measurements (cf. Fig. 4) discovered the overdamped A_1(LO) mode vanishing in the background – consistent with a recent study using RSS [62]. Recognizing the fact that the PLP mode is associated with ω_P – this observation is useful for assessing charge carrier concentration by fitting the observed A_1(LO) Ram an profile using: [60]

$$I(\omega) \propto A(\omega) Im\left[-\frac{1}{\varepsilon(\omega)}\right] \quad (4)$$

where $A(\omega)$is expressed as:

$$A(\omega) = 1 + 2C\frac{\omega_T^2}{\Delta}[\omega_P^2\gamma(\omega_T^2 - \omega^2) - \omega^2\Gamma(\omega^2 + \gamma^2 - \omega_P^2)] + C^2 \left(\frac{\omega_T^4}{\Delta(\omega_L^2 - \omega_T^2)}\right)\{\omega_P^2[\gamma(\omega_L^2 - \omega_T^2) + \Gamma(\omega_P^2 - \omega^2)] + \omega^2\Gamma(\omega^2 + \gamma^2)\} \quad (5)$$

with

$$\Delta = \omega_P^2\gamma[(\omega_T^2 - \omega^2)^2 + \omega^2\gamma^2] + \omega^2\Gamma(\omega_L^2 - \omega_T^2)(\omega^2 + \gamma^2) \quad (6)$$

Here, the terms ω_T and ω_L represent the unstrained A_1(TO) = 533 cm^{-1} and A_1(LO) = 734 cm^{-1} phonon frequencies; γ and Γ are the plasmon and phonon damping constants, respectively;

Table 3
Parameter values used in fitting Raman spectral profiles of (*a*) $E_2^{high}(GaN)$ mode with Eq. (1) and (*b*) A_1(LO) mode with Eqs. (4–6) for Si-doped MOCVD grown GaN/ Sapphire samples having different film thickness and carrier concentration (see: text).

Sample #	N (10^{17}) cm^{-3}	$E_2^{high}(GaN)peak$ [a]	A (cm^{-1}) [a]	Γ(cm^{-1}) [a]	L (Å) [a]	Raman Shift cm^{-1}	Dominant mode in A_1(LO) Raman profile [a]
S_1	3.58	569.3	569.4	5.0	20.0	739	A_1(LO)
S_2	6.57	568.8	569.7	4.8	20.0	750	E_g (Sapphire)
S_3	4.85	569.5	570.0	5.0	16.0	740	A_1(LO)
S_4	7.65	569.5	569.8	5.0	16.0	750	E_g (Sapphire)
S_5	2.77	569.0	570.0	5.0	20.0	738	A_1(LO)

[a] This work.

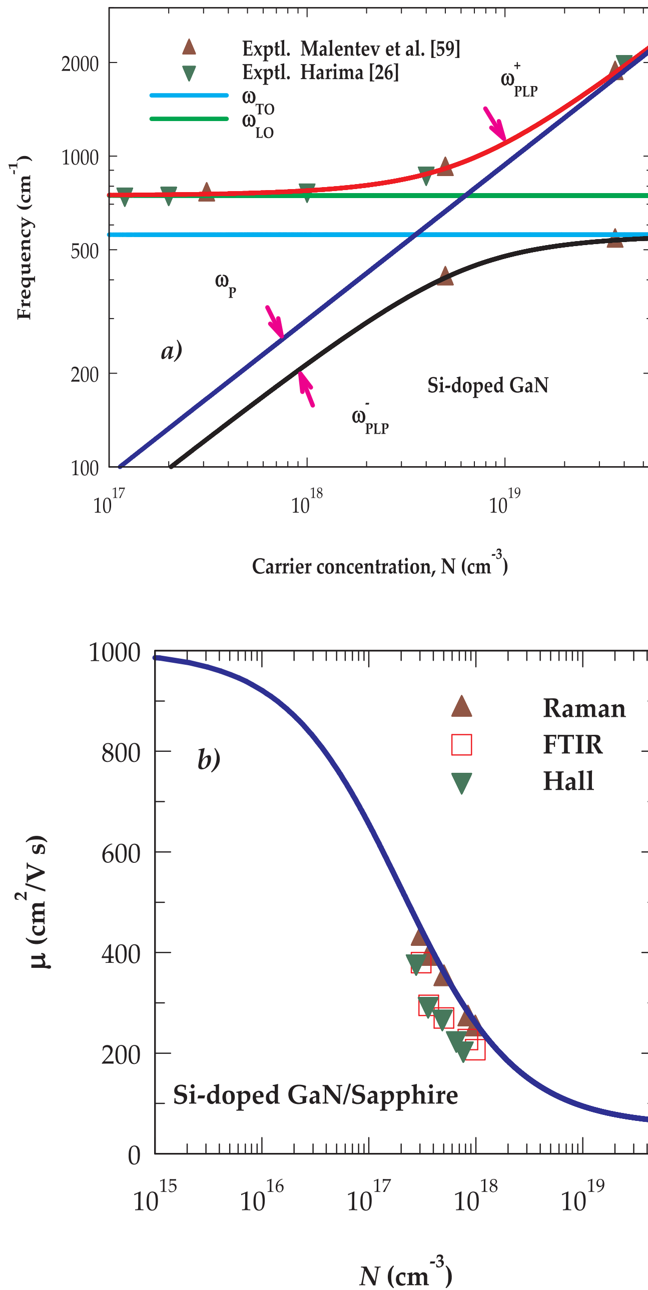

Fig. 6. (*a*) The carrier-density dependence of plasmon-LO-phonon modes ($L_\pm$) in Si-doped GaN using Eq. (3). The experimental results are from Harima Ref. [26] and Malentev et al. [59]. (*b*) Comparison of the experimental (Raman, FTIR and Hall) carrier-density dependence electron mobility μ in Si-doped GaN with Caughey – Thomas model Ref. [47] (see text).

and $C = 0.48$ is the so-called Faust-Henry coefficient [63].

By incorporating Eqs. (4–6), we have simulated Raman intensity profiles of A_1(LO) mode for each Si-doped GaN/Sapphire sample by meticulously including contributions from the plasmon-LO-phonon couplings and Lorentzian shaped E_g sapphire modes (see: Table 3). In this process, a Markovian least square fitting procedure is adopted with $m^* = 0.2\, m_e$, $\varepsilon_\infty = 5.35$, $\gamma = \frac{e}{m^*\mu}$ as input while fine tuning the values of γ, Γ and ω_P. Although the estimated results of N and μ from the line shape fits are somewhat different from our Hall measurements and recent FTIR spectral analyses [64] (cf. Table 1), the values agreed, however, reasonably well with an empirical Caughey – Thomas model [47] (see: Fig. 6 *b*)). Our best fit calculations of the Raman profiles displayed in Fig. 7 *a*)- *e*) compared favorably well with the experimental data. These findings clearly suggested that a careful analysis of the RSS data can be valuable for estimating transport parameters in Si-doped GaN/Sapphire and/or other semiconductors.

3.2.3. Impurity-induced vibrational modes

Both IR and Raman scattering spectroscopy are frequently used to acquire impurity vibrational modes for comprehending the site selectivity of isolated and/or complex defect centers in doped semiconductors [65]. Like III-V compounds, one expects observing defect modes of light impurities in III-Ns to appear either in the phonon gap (as gap modes) and/or above the maximum phonon ω_{max} frequency region (as LVMs). Despite a few experimental attempts, [27,28] no LVMs are ascribed to the isolated defects (C_N, O_N, Si_{Ga}, Mg_{Ga}) in GaN. It is quite likely that these defects could have induced static disorder and/or activated forbidden modes. Therefore, a careful analysis of the dynamical properties of doped GaN is very much needed to help appraise the observed Raman features and assess the site selectivity of defects.

By using a Green's function (GF's) methodology [65,66] we have simulated the structural and dynamical properties of GaN doped with Mg_{Ga} (a^-), and Si_{Ga} (d^+). Impurity vibrational modes of isolated defects in different irreducible representations (μΓ) are obtained by solving the real part of the determinant: [65]

$$\prod_{\mu\Gamma} \{det|\mathbf{I} - \mathbf{G^o}_{\mu\Gamma}\mathbf{P}_{\mu\Gamma}|\} = 0 \tag{7}$$

where $\mathbf{P}$ is the perturbation matrix of isolated defects and $\mathbf{G^o}$ represent the GF's matrix elements of perfect GaN lattice. For calculating the impurity modes of defects occupying Ga site in GaN, one needs the perturbation matrix $\mathbf{P}$ with mass change parameter (ε_1) and force constant change parameter (t), as well as $\mathbf{G^o}$. Here, we have used the rigid-ion-model (RIM) [48] fitted phonons to IXS data [50] for calculating the GF's matrix elements of GaN. For $\mathbf{P}$ the force constant change parameters of Mg_{Ga} (a^-), and Si_{Ga} (d^+) defects are obtained from the lattice relaxation of each defect in GaN by using second derivatives of the total energies estimated from the first-principle bond-orbital model (BOM) [66]. Consistent with the local density functional [2] theory, our BOM results have provided contraction (inward relaxation) in the bond length for Si_{Ga} (d^+) and stretching (outward relaxation) for Mg_{Ga} (a^-) defects in GaN.

With the appropriate values of force variations of $^{28}Si_{Ga}$ (stiffening) and $^{24}Mg_{Ga}$ (softening) in GaN, the simulated results of the impurity activated modes are reported in Table 4. Despite the differences in the impurity-host bonding, the mass change parameters in the two cases have justified the comparable values of the calculated and experimentally [27] observed phonon features. One must note that the lighter isolated Si and Mg defects occupying Ga sites could have produced discrete LVMs above the maximum phonon ω_m (~742 cm^{-1}) frequency of GaN. As some of the simulated IVMs (see: Table 4) appear below A_1(LO) mode at nearly closest frequency range independent of the atomic masses – clearly suggest that such features cannot be related to the LVMs but instead to defect-activated vibrational modes.

4. Summary and conclusions

In summary, we have reported the results of a comprehensive experimental and theoretical study to examine the vibrational and structural properties of high quality, Si doped GaN/Sapphire epifilms prepared by the two-step MOCVD growth technique. For an undoped 3.6 µm thick sample (# S_0) our polarized micro-Raman measurements have not only provided major 1st order Raman active modes of GaN epifilm but also sapphire substrate. Careful analysis of the 2nd-order Raman spectra using critical-point-phonon energies from RIM [48] fitted IXS data [50] with applicable group-theoretic selection rules have helped us attain expedient information of the lattice dynamics of GaN. In Si-doped GaN/Sapphire samples (# S_1-S_5) a modified PCM is used for simulating the Raman line shapes of E_2^{high} phonons for monitoring both

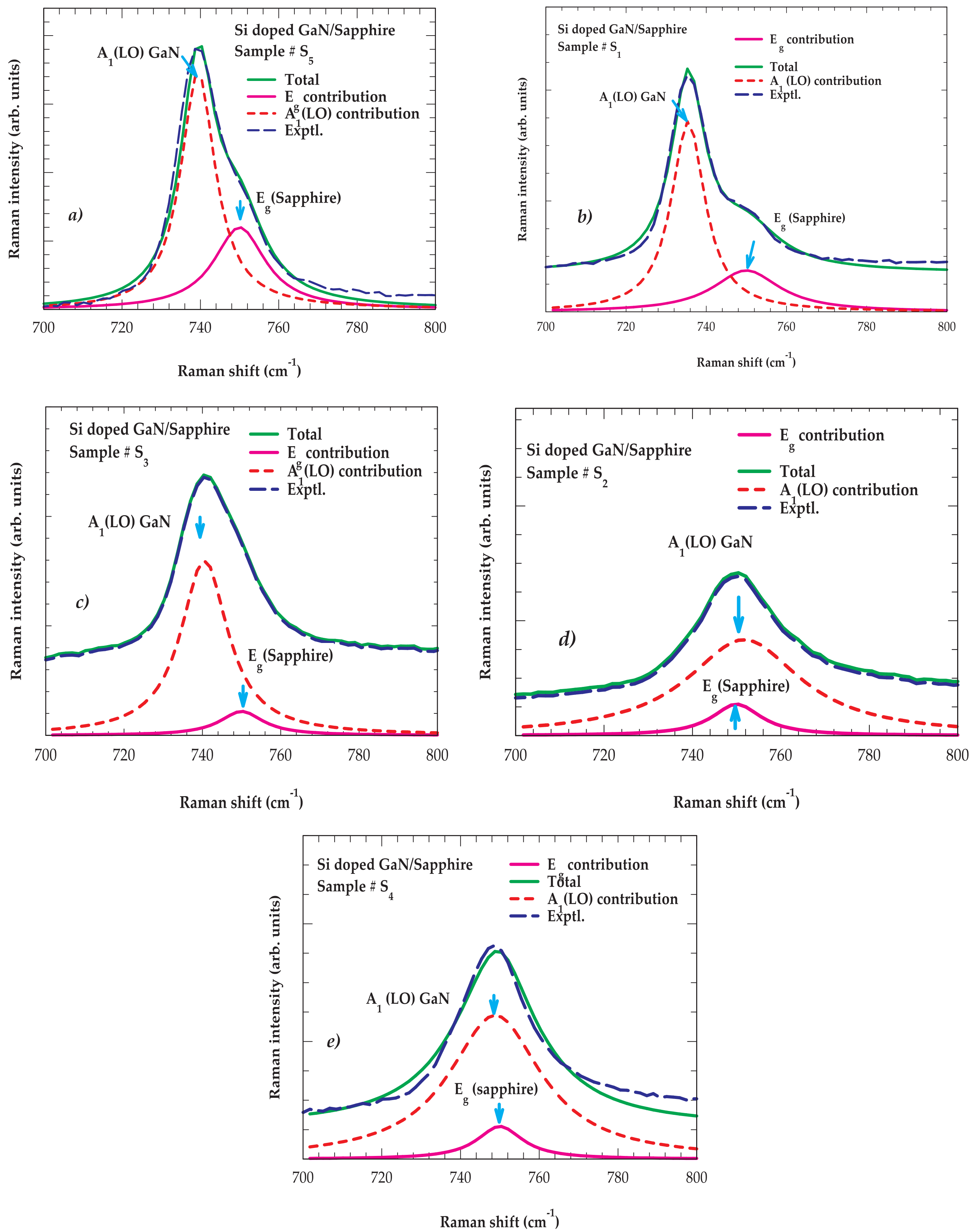

Fig. 7. The fitting of Raman scattering spectra of A_1(LO) mode for each sample (a-e) by using Eqs. (4–6) with parameter values from Table 3 (see text).

Table 4
Comparison of lattice dynamical calculations with Raman scattering results of impurity-vibrational modes for $^{28}Si_{Ga}$ and $^{24}Mg_{Ga}$ in GaN (see text).

System	Defect	Impurity vibrational modes (cm^{-1})						
GaN								
	Si_{Ga}			300 [a)]	420 [a)]		670 [a)]	
		135 (A_1)*	287(A_1)*	306(A_1)*			658(A_1)*	720 (A_1)*
				317 (E)*				727 (E)*
	Mg_{Ga}			300 [a)]	420 [a)]		670 [a)]	
		136[b)]	262[b)]	320[b)]		595[b)]	656[b)]	
			260[c)]				657[c)]	
		130 (A_1)*	270 (A_1)*	304(A_1)*			652 (A_1)*[b)]	718(A_1)*
				315 (E)*				723 (E)*

*Our calculations.
[a-c)] Ref. [27–28].

the crystalline quality and strain state. In samples with $N < 9.95 \times 10^{17}$ cm^{-3}, our study has perceived no appreciable shift in the E_2^{high} mode – suggesting a trivial residual strain caused by Si dopants in GaN films. In lightly doped samples, while the optical GaN modes are coupled to the electron plasma – an over-damped A_1(LO) mode has vanished in the background at higher N. In each sample, we estimated the transport parameters by simulating Raman profiles of the A_1(LO) modes with contributions from plasmon-LO-phonon coupling and Lorentzian shaped E_g sapphire mode. While our values of N andμ obtained from the Raman line shape fits are slightly higher than those of the Hall and FTIR spectral analyses data [64] – they, however, agreed reasonably well with the empirical Caughey–Thomas model [47]. By using a realistic GF's theory, we also calculated the impurity vibrational modes of Si donors and Mg acceptors in GaN using [65] a RIM phonons [48] fitted to the IXS data and including force constant change parameters estimated from the first-principle BOM [66]. Despite the differences in impurity-host bonding – the mass change parameters in the two cases justified comparable values of the calculated and experimentally observed phonon frequencies [27,28]. Earlier Limmer et al. [58] and Lee et al. [57] ascribed the Raman peaks [28] near ~420 and 670 cm^{-1} as the vibrational modes of vacancy-related defects resulting from the implantation-induced damage of n-type GaN. Similar features have also been observed in the 2nd order RSS and assigned to overtones of transverse acoustic phonons. Consistent with Raman studies, [27] our calculations suggest the possibilities of impurity activated acoustic modes between 130 and 135 cm^{-1}, 270 to 287 cm^{-1}, 304 to 317 cm^{-1} and the optic modes between 652 and 658 cm^{-1} and 717 to 727 cm^{-1} – with no evidence of gap and/or LVMs of Mg and Si defects in GaN. More FTIR absorption and RSS studies are underway to assess the chemical origin of different donor (Ge_{Ga}, O_N) and acceptor (C_N, Be_{Ga}, Zn_{Ga}) species in GaN – observing their vibrational traits and exploiting them as spectroscopic fingerprints in realistic lattice dynamical simulations. We strongly feel that studying such material characteristics for both n- and p-doped GaN epifilms is essential for scientists to evaluate their potential use in designing and/or engineering electronic devices of various industrial applications.

Declaration of Competing Interest

The authors declare that they have no known competing financial interests or personal relationships that could have appeared to influence the work reported in this paper.

Acknowledgements

One of us (DNT) is thankful to Dr. Deanne Snavely, the Dean of the College of natural sciences and mathematics (C-NSM) at Indiana University of Pennsylvania for travel support and to the Graduate school for the award of an Innovation grant. ZCF acknowledges partial financial support from the State Key Laboratory of Luminescence and Applications, Chinese Academy of Sciences (# SKLA-2019-06). HH Lin acknowledges financial support from the Ministry of Science and Technology, Taiwan, under the contract #MOST 108-2221-E-002-013-MY3.

References

[1] P. Fay, D. Jena, P. Maki (Eds.), High-Frequency GaN Electronic Devices, Springer, 2020.
[2] J. Chen, J. Zhu, J. Ning, X. Duan, D. Wang, J. Zhang, Y. Hao, Strong selective oxidization on two-dimensional GaN: a first principles study, Phys. Chem. Chem. Phys. 21 (2019) 6224.
[3] Y. Wang, GaN-Based Schottky Diode, http://dx.doi.org/10.5772/intechopen.77024.
[4] H. Amano, et al., The 2018 GaN power electronics roadmap, J. Phys. D: Appl. Phys. 51 (2018) 163001.
[5] I. Lo, Advances in GaN crystals and their applications, Crystals 8 (2018) 117.
[6] K. Bern, https://www.renesas.com/us/en/doc/whitepapers/rad-hard/advantages-of-using-gan-fets-in-satellite-applications.pdf.
[7] Ó.M. Rodríguez-Benítez, M. Ponce-Silva, L.H. González, J.A. Aquí-Tapia, A.C. Sánchez, G.C. Lara, C. Cortés-García, Recent Advance and Future Progress of GaN Power Semiconductor Devices used in PV Module Integrated Converters, 10.20944/preprints 2018,12,0072.v1.
[8] Y. Arakawa, K. Ueno, H. Imabeppu, A. Kobayashi, J. Ohta, H. Fujioka, Electrical properties of Si-doped GaN prepared using pulsed sputtering *Appl*, Phys. Lett. 110 (2017) 042103.
[9] T. Flack, B.N. Pushpakaran, S. Bayne, GaN technology for power electronic applications: a review, J. Electronic Mater. 45 (2016) 2673.
[10] Y. Cao, R. Chu, R. Li, M. Chen, R. Chang, B. Hughes, High barrier height GaN Schottky diodes: Pt/GaN and Pd/GaN, Appl. Phys. Lett. 108 (2016) 062103.
[11] K. Ueno, A. Kobayashi, H. Fujioka, Characteristics of unintentionally doped and lightly Si-doped GaN prepared via pulsed sputtering, AIP Adv. 9 (2019) 075123, https://doi.org/10.1063/1.5103185.
[12] Z. Hu, K. Nomoto, B. Song, M. Zhu, M. Qi, M. Pan, X. Gao, V. Protasenko, D. Jena, H.G. Xing, Near unity ideality factor and Shockley-Read-Hall lifetime in GaN-on-GaN *p-n* diodes with avalanche breakdown, Appl. Phys. Lett. 107 (2015) 243501.
[13] S. Fujita, Wide-bandgap semiconductor materials: For their full bloom, Jpn. J. Appl. Phys. 54 (2015) 030101.
[14] N. Tanaka, K. Hasegawa, K. Yasunishi, N. Murakami, T. Oka, 50 A vertical GaN Schottky barrier diode on a free-standing GaN substrate with blocking voltage of 790 V, Appl. Phys. Express 8 (2015) 071001.
[15] T. Oka, T. Ina, Y. Ueno, T. Ina, K. Hasegawa, Vertical GaN-based trench metal oxide semiconductor field-effect transistors on a free-standing GaN substrate with blocking voltage of 1.6 kV, Appl. Phys. Express 7 (2014) 021002.
[16] Y. Saitoh, K. Sumiyoshi, M. Okada, T. Horii, T. Miyazaki, H. Shiomi, M. Ueno, K. Katayama, M. Kiyama, T. Nakamura, Extremely low on-resistance and high breakdown voltage observed in vertical GaN Schottky barrier diodes with high mobility drift layers on low-dislocation-density GaN substrates, Appl. Phys. Exp. 3 (2010) 081001.
[17] S.J. Pearton, C.R. Abernathy, G.T. Thaler, R.M. Frazier, D.P. Norton, F. Ren, Y.D. Park, J.M. Zavada, I.A. Buyanova, W.M. Chen, A.F. Hebard, Wide bandgap GaN-based semiconductors for spintronics, J. Phys.: Condens. Matter 16 (2004) R209.
[18] K. Ueno, E. Kishikawa, S. Inoue, J. Ohta, H. Fujioka, M. Oshima, H. Fukuyama, Improved resistive switching phenomena observed in SiN_x-based resistive switching memory through oxygen doping process, Phys. Status Solidi RRL 8 (2014) 256.
[19] E. Nakamura, K. Ueno, J. Ohta, H. Fujioka, M. Oshima, Dramatic reduction in process temperature of InGaN-based light-emitting diodes by pulsed sputtering growth technique, Appl. Phys. Lett. 104 (2014) 051121.
[20] J.W. Shon, J. Ohta, K. Ueno, A. Kobayashi, H. Fujioka, Fabrication of full-color InGaN-based light-emitting diodes on amorphous substrates by pulsed sputtering, Sci. Rep. 4 (2014) 5325.
[21] T. Watanabe, J. Ohta, T. Kondo, M. Ohashi, K. Ueno, A. Kobayashi, H. Fujioka,

AlGaN/GaN heterostructure prepared on a Si (110) substrate *via* pulsed sputtering, Appl. Phys. Lett. 104 (2014) 182111.
[22] J.T. Chen, U. Forsberg, E. Janzen, Impact of residual carbon on two-dimensional electron gas properties in $Al_xGa_{1-x}N$/GaN heterostructure, Appl. Phys. Lett. 102 (2013) 193506.
[23] A. Dadgar, J. Bläsing, A. Diez, and A. Krost, Crack-Free, Crack-Free, Highly Conducting GaN Layers on Si Substrates by Ge Doping, Appl. Phys. Express 4 (2011) 011001.; S. Fritze, A. Dadgar, H. Witte, M. Bügler, A. Rohrbeck, J. Bläsing, A. Hoffmann, and A. Krost, High Si and Ge n-type doping of GaN doping-Limits and impact on stress, Appl. Phys. Lett. 100 (2012) 122104.
[24] Hiroshi Amano, Nobel Lecture, December 8, 2014; H. Amano, N. Sawaki, I. Akasaki, and Y. Toyada, Metalorganic vapor phase epitaxial growth of a high quality GaN film using an AlN buffer layer, Appl. Phys. 48 (1986) 353.
[25] S. Nakamura, T. Mukai, and M. Senoh, Si- and Ge-Doped GaN Films Grown with GaN Buffer Layers, Jpn. J. Appl. Phys. 31 (1992) 2883.; S. Nakamura, T. Mukai, and M. Senoh, Candela-class high-brightness InGaN/AlGaN double-heterostructure blue-light-emitting diodes, Appl. Phys. Lett. 64 (1994) 1687.; S. Nakamura, M. Senoh, S. Nagahama, T. Yamada, and T. Mukai, Superbright Green InGaN Single-Quantum-Well-Structure Light-Emitting Diodes, Jpn J. Appl. Phys. 34 (1995) L1332.
[26] H. Harima, Properties of GaN and related compounds studied by means of Raman scattering, J. Phys.: Condens. Matter 14 (2002) R967–R993.
[27] M. Katsikini, K. Papagelis, E. C. Paloura, and S. Ves, Raman study of Mg, Si, O, and N implanted GaN, J. Appl. Phys. 94 (2003) 4389.; M. Katsikini, F. Pinakidoua, J. Arvanitidis, E.C. Paloura, S. Ves, Ph. Komninou, Z. Bougrioua, E. Iliopoulos, and T. D. Moustakas, Comparison of Fe and Si doping of GaN: An EXAFS and Raman study, Mat. Sci. Eng. B 176 (2011) 723-726.
[28] G. Kaczmarczyk, A. Kaschner, A. Hoffman and C. Thomsen, Impurity-induced modes of Mg, As, Si, and C in hexagonal and cubic GaN, Phys. Rev. B 61 (2000) 5353.; A. Kaschner, H. Siegle, A. Hoffmann, and C. Thomsen, Influence of doping on the lattice dynamics of gallium nitride, MRS Internet J. Nitride Semicond. Res. 4S1 G3 (1999) 57.
[29] Z. Xu, Z. He, Y. Song, X. Fu, M. Rommel, X. Luo, A. Hartmaier, J. Zhang, and F. Fang, Application of Raman Spectroscopy Characterization in Micro/Nano-Machining, Micro-machines, 9 (2018) 361.; doi:10.3390/mi9070361.
[30] W. S. Li, Z. X. Shen, Z. C. Feng, and S. Chua, Temperature dependence of Raman scattering in hexagonal gallium nitride films J. Appl. Phys. 87 (2000) 3332.; Z. C. Feng, W. Wang, S. J. Chua, P. X. Zhang, K. P. J. Williams, and G. D. Pitt, Raman scattering properties of GaN thin films grown on sapphire under visible and ultra-violet excitation, J. Raman Spectr. 32 (2001) 840-846; Z. C. Feng, Opt. Eng. 41 (2002) 2022.
[31] Y.L. Wu, Z.C. Feng, J.-F. Lee, W. Tong, B.K. Wagner, I. Ferguson, and Weijie Lu, X-ray absorption and Raman study of GaN films grown on different substrates by different techniques, Thin Solid Films 518 (2010) 7475–7479.
[32] B.I. Tsykaniuk, A.S. Nikolenko, V.V. Strelchuk, V.M. Naseka, Y.I. Mazur, M.E. Ware, E.A. DeCuir Jr, B. Sadovyi, J.L. Weyher, R. Jakiela, G.J. Salamo, A.E. Belyaev, Infrared reflectance analysis of epitaxial n-type doped GaN layers grown on sapphire, Nanoscale Res Lett. 12 (2017) 397.
[33] M.J. Deen, F. Pascal, Electrical Characterization of Semiconductor Materials and Device, Ch. 20, in: S. Kasap, P. Capper (Eds.), Handbook of Electronic and Photonic Materials, Springer, 2017.
[34] M. Lee, T.K.O. Vu, K.S. Lee, E.K. Kim, S. Park, Electronic states of deep trap levels in a-plane GaN templates grown on r-plane sapphire by HVPE, Sci Rep. 8 (2018) 7814.
[35] T. Kogiso, T. Narita, H. Yoshida, Y. Tokuda, K. Tomita, and T. Kachi, Frontiers of Nitride Semiconductor Research, Jap. J. Appl. Phys. 58 (2019) SCCB36.
[36] E.F. Schubert, I.D. Goepfert, W. Grieshaber, J.M. Redwing, Optical properties of Si-doped GaN, Appl. Phys. Lett. 71 (1997) 921.
[37] T.Y. Lin, W.S. Su, W.S. Su, Y.F. Chen, Investigation of surface properties of Si-doped GaN films by electric force microscopy and photoluminescence, Sol. Stat. Commun. 130 (2004) 49.
[38] L.T. Tung, K.L. Lin, E.Y. Chang, W.C. Huang, Y.L. Hsiao, C.H. Chiang, Photoluminescence and Raman studies of GaN films grown by MOCVD, J. Phys: Conf. Ser. 187 (2009) 012021.
[39] F.J. Xu, B. Shen, L. Lu, Z.L. Miao, J. Song, Z.J. Yang, G.Y. Zhang, X.P. Hao, B.Y. Wang, X.Q. Shen, H. Okumura, Different origins of the yellow luminescence in as-grown high-resistance GaN and unintentional-doped GaN films, J. Appl. Phys. 107 (2010) 023528.
[40] H. Yamada, H. Chonan, T. Takahashi, T. Yamada, M. Shimizu, Deep-level traps in lightly Si-doped nGaN on free-standing m-oriented GaN substrates, AIP Adv. 8 (2018) 045311.
[41] F. Liang, D. Zhao, D. Jiang, Z. Liu, J. Zhu, P. Chen, J. Yang, S. Liu, Y. Xing, L. Zhang, Role of Si and C Impurities in Yellow and Blue Luminescence of Unintentionally and Si-Doped, GaN, 10262018, Nanomaterials 8 (2018), https://doi.org/10.3390/nano8121026.
[42] Y. Huang, X.D. Chen, S. Fung, C.D. Beling, C.C. Ling, Z.F. Wei, S.J. Xu, C.Y. Zhi, The depth-profiled carrier concentration and scattering mechanism in undoped GaN film grown on sapphire, J. Appl. Phys. 96 (2004) 1120.
[43] K. Ishioka, K. Kato, N. Ohashi, H. Haneda, M. Kitajima, H. Petek, The effect of n-and p-type doping on coherent phonons in GaN, J. Phys.: Condens. Matter 25 (2013) 205404.
[44] E. Richter, T. Stoica, U. Zeimer, C. Netzel, M. Weyers, G. Tränkle, Si doping of GaN in hydride vapor-phase epitaxy, J. Electron. Mater. 42 (2013) 820.
[45] A. Kasic, M. Schubert, S. Einfeldt, D. Hommel, T.E. Tiwald, Effects of the narrow band gap on the properties of InN, Phys. Rev. B 62 (2002) 7365.
[46] J.-L. Farvacque, Z. Bougrioua, I. Moerman, G. Van Tendeloo, O. Lebedev, Role of the defect microstructure on the electrical transport properties in undoped and Si-doped GaN grown by LP-MOVPE, Physica B 273–274 (1999) 140143.
[47] D.M. Caughey, R.E. Thomas, Carrier mobilities in silicon empirically related to doping and field, Proc. IEEE 55 (1967) 2192.
[48] W.G. Hong, Z. Jian, Z.K. Ming, X.X. De, Lattice dynamics of wurtzite semi-conductors GaN and AlN, Acta Phys. Sinica 7 (1998) 841.
[49] H. Siegle, G. Kaczmarczyk, L. Filipidis, A. P. Litvinchuk, A. Hoffman, and C. Thomsen, Zone-boundary phonons in hexagonal and cubic GaN, Phys. Rev. B 55 (1997) 7000.; V. Y. Davydov, Y. E. Kitaev, I. N. Goncharuk, A. N. Simirnov, J. Graul, O. Semchinova, D. Uffmann, M. B. Smirnov, A. P. Mirgorodsky, and R. A. Evarestov, Phonon dispersion and Raman scattering in hexagonal GaN and AlN, Phys. Rev. B 58 (1998) 12899.
[50] T. Ruf, J. Serrano, M. Cardona, P. Pavone, M. Pabst, M. Krisch, M. D'Astuto, T. Suski, I. Grzegory, M. Leszczynski, Phonon Dispersion Curves in Wurtzite-Structure GaN Determined by Inelastic X-Ray Scattering, Phys. Rev. Lett. 86 (2001) 906.
[51] H. Richter, Z.P. Wang, L. Ley, The one phonon Raman spectrum in microcrystalline silicon, Sol. State Commun. 39 (1981) 625.
[52] P. Parayanthal, F.H. Pollak, Raman scattering in alloy semiconductors:“ spatial correlation” model, Phys. Rev. Lett. 52 (1984) 1822.
[53] I.H. Cambell, P.M. Fauchet, The effects of microcrystal size and shape on the one phonon Raman spectra of crystalline semiconductors, Sol. State Commun. 58 (1986) 739.
[54] A. Fischer, L. Anthony, A.D. Compaan, Raman analysis range clustering in laser-deposited films, Appl. Phys. Lett. 72 (1998) 2559.
[55] A.K. Arora, M. Rajalakshmi, T.R. Ravindran, V. Sivasubramanian, Raman spectroscopy of optical phonon confinement in nanostructured materials, J. Raman Spectrosc. 38 (2007) 604.
[56] L. Bergman, M.D. Bremser, W.G. Perry, R.F. Davis, M. Dutta, R.J. Nemanich, Raman analysis of the configurational disorder in films, Appl. Phys. Lett. 71 (1997) 2157.
[57] I. Lee, I. Choi, C. Lee, E. Shin, D. Kim, S.K. Noh, S. Son, K.Y. Lim, H.J. Lee, Stress relaxation in Si-doped GaN studied by Raman spectroscopy, J. Appl. Phys. 83 (1998) 5787.
[58] W. Limmer, W. Ritter, R. Sauer, B. Mensching, C. Liu, B. Rauschenbach, Raman scattering in ion-implanted GaN, Appl. Phys. Lett. 72 (1998) 2589.
[59] G.A. Melentev, D. Yu Yaichnikov, V.A. Shalygin, M. Ya Vinnichenko, L.E. Vorobjev, D.A. Firsov, L. Riuttanen, S. Suihkonen, Plasmon phonon modes and optical resonances in *n*-GaN, J. Phys: Conf. Series 690 (2016) 012005.
[60] K. Jeganathan, R.K. Debnath, R. Meijers, T. Stoica, R. Calarco, D. Grützmacher, H. Lüth, Raman scattering of phonon-plasmon coupled modes in self-assembled GaN nanowires, J. Appl. Phys. 105 (2009) 123707.
[61] E. Richter, T. Stoica, U. Zeimer, C. Netzel, M. Meyers, G. Trankle, Si doping of GaN in hydride vapor-phase epitaxy, J. Electron. Mater. 42 (2013) 820.
[62] M. Katsikini, F. Pinakidou, J. Arvanitidis, E.C. Paloura, S. Ves, P. Komninou, Z. Bougrioua, E. Iliopoulos, Comparison of Fe and Si doping of GaN: An EXAFS and Raman study, Mat. Sci. Eng. B176 (2011) 723.
[63] W.L. Faust, C.H. Henry, Relaxation time, effective mass, and structure of ions in liquid helium, Phys. Rev. Lett. 17 (1966) 1265.
[64] D. N. Talwar, H. H. Lin, Z. C. Feng, Polarization dependent infrared reflectivity studies of Si-doped MOCVD grown GaN/Sapphire epilayers, Mat. Chem. Phys. (in press).
[65] D.N. Talwar, H.H. Lin, Z.C. Feng, Phonon characteristics of Si-doped InAs grown by gas-source molecular beam epitaxy, J. Raman Spectrosc. 50 (2019) 1731–1743.
[66] D.N. Talwar, Dilute III-V Nitride Semiconductors and Material Systems—Physics and Technology, Ch. 9, in: A. Erol (Ed.), Springer Series in Materials Science, Springer-Verlag, Berlin, 2008, p. 222.